Applied Catalysis B: Environmental 140–141 (2013) 233–240

Contents lists available at SciVerse ScienceDirect

Applied Catalysis B: Environmental

journal homepage: www.elsevier.com/locate/apcatb

Lithium ion-inserted TiO_2 nanotube array photoelectrocatalysts

Unseock Kang, Hyunwoong Park*

School of Energy Engineering, Kyungpook National University, Daegu 702-701, South Korea

ARTICLE INFO

Article history:
Received 18 January 2013
Received in revised form 25 March 2013
Accepted 1 April 2013
Available online 8 April 2013

Keywords:
Photoelectrochemical
Photoelectrocatalytic
Charge separation
IPCE
Solar fuels

ABSTRACT

A quick electrochemical Li ion insertion into TiO_2 nanotube arrays (TNTs) markedly enhances the photoelectrochemical and photoelectrocatalytic performance. Potential pulses ($-1.0 \sim -1.7\ V_{SCE}$ for 1–11 s in 1 M $LiClO_4$) to pre-annealed TNTs effectively insert Li ions (pre-annealed Li-TNTs) into the mouth/wall and bottom TiO_2 depending on the insertion condition. Pre-annealed Li-TNTs prepared under an optimal Li ion insertion condition ($-1.4\ V_{SCE}$ for 3 s) exhibit ~70%-enhanced photocurrent generation, ~2.5 fold-higher incident photon-to-current efficiency, and an improved photoelectrocatalytic activity for the degradation of phenolic compounds in 1 M KOH electrolyte. A change in photoluminescence (PL) emission spectra and decrease in charge transfer resistance by Li ion insertion suggest that the inserted Li ions play a role in inhibiting charge recombination by compensating for the photogenerated Ti^{3+} charges (Li^+-Ti^{3+}-OH). However, as KOH concentration is diluted such enhanced Li^+ effects gradually vanish primarily due to liberation of reversibly inserted Li ions. To insert Li ions irreversibly, the potential pulses were applied to non-annealed TNTs followed by annealing (post-annealed Li-TNTs). Comparison between pre-annealed and post-annealed Li-TNTs in circum-neutral pH (0.1 M Na_2SO_4 at pH ~6) indicates that the former exhibits a similar performance to bare TNTs (absence of Li ion effect), whereas the latter shows a superior performance with ca. 2.5-fold higher photoelectrochemical and photoelectrocatalytic activities. Detailed surface analyses (XPS, XRD, PL, SEM, ICP-MS, etc.) and Li^+-induced reaction mechanism were discussed.

1. Introduction

TiO_2 nanotube arrays (TNTs) grown on titanium foil through electrochemical anodization have attracted great attention as a light harvesting 1-D scaffold [1,2]. The self-standing, aligned 1-D architecture is beneficial for photogenerated electron transport along the tube framework leaving holes on the surface [1,3–6]. In addition, the tubular structure provides a unique submicron-sized environment where a variety of metals, semiconductors, and molecules are selectively located for a further increase in the photoelectrochemical performance and various applications [7–12]. Despite such geometric uniqueness and photoelectrocatalytic superiority compared to TiO_2 nanoparticles (TNPs), however, TNTs still suffers from inherent charge recombination [4,10,13–15], limiting their further application Scheme 1.

Recently, Li ion insertion into TiO_2 has received growing attention since the Li-battery industry has rapidly grown [16–21]. The insertion is simply achieved by applying negative potentials to TiO_2 electrodes in a Li^+-rich solution (reaction (1)):

$$> TiO_2 + xe^- + xLi^+ \rightarrow > Li_xTiO_2 \quad (1)$$

A sufficiently high negative bias potential supplies excess electrons to the TiO_2 conduction band (CB) increasing capacitance and conductivity [22], as well as inducing upward band-bending and an accumulation regime in TiO_2. The accumulation of negative charges (i.e., $)Ti^{3+}$-OH) is then effectively compensated by Li^+ insertion ($)Ti^{3+}Li^+$-OH) [20]. A crystallographic study estimated that there are channels with a minimum diameter of 0.07 nm in TiO_2 [23], making Li ion (ionic diameter ~ 0.068 nm) insertion inherently possible. Electrochemical Li ion insertion is favored by small and anatase TiO_2 particles [24,25], and creates new Ti 2p states (Ti^{3+}) along with changed O1s states due to the formation of Li_2O/LiOH [26]. Treatment of TiO_2 with Li ions shifts the Fermi level (E_F) upward due to the lithium oxide/hydroxide dipole layers ($)Ti-O^-$-Li^+), improving the photovoltages in dye-sensitized solar cells [27].

It is surprising that despite a number of papers on Li^+-inserted TiO_2 (Li-TiO_2), its photoelectrocatalytic behavior has been hardly reported. Very recently, Meekins and Kamat showed that Li ion insertion significantly enhances the photoelectrochemical efficiency of TNTs in highly Li^+-rich or alkaline solutions [28]. The high efficiency Li-TNTs was attributed primarily to inhibited charge recombination by blocking electron trap sites. Two challenging issues remain unsolved. Firstly, if the enhanced photoelectrochemical efficiency truly resulted from the Li^+-inhibited charge recombination, hole-mediated photocatalytic activities also should be enhanced because the inhibited charge recombination should

* Corresponding author. Tel.: +82 53 950 8973.
E-mail address: hwp@knu.ac.kr (H. Park).

0926-3373/$ – see front matter © 2013 Elsevier B.V. All rights reserved.
http://dx.doi.org/10.1016/j.apcatb.2013.04.003

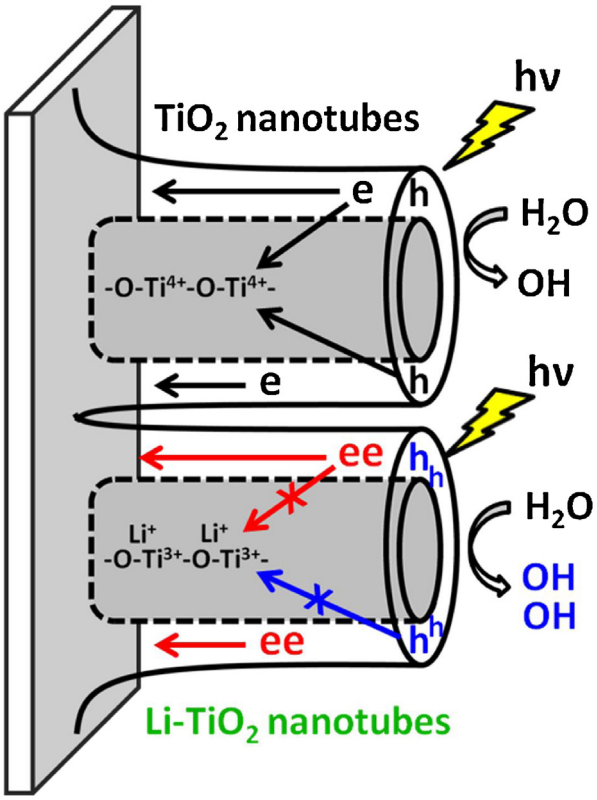

Scheme 1. Schematic illustration of photogenerated charge transfers in bare and Li ion-inserted TiO_2 nanotube arrays.

result in more generation of holes (or hydroxyl radicals). However, contrary results were reported by other groups that the photocatalytic activity of Li-TiO_2 particles is decreased for the decomposition of organic chemicals [29,30]. Secondly, the photoelectrochemical stability of Li-TNTs must be guaranteed for practical application. Unfortunately, the inserted Li ions tend to leach out from TNTs at circum-neutral and acidic pH because protons competes with Li ions for TNTs.

The objective of this study is to investigate if Li ion insertion enhances photoelectrochemical charge transfers occurring on TNTs, and as a result, increases its photoelectrocatalytic performance for degradation of organic compounds. For this objective, Li ions are inserted in TNTs in pre-annealed TNTs. Because this type of TNTs is crystallized prior to Li ion insertion, the post-inserted Li ions are exchangeable with protons (i.e., reversible Li^+ insertion) and preserved in the TNTs only in alkaline conditions (see reaction (4)). The Li ion effects are found to be very promising for photocurrent generation and photoelectrocatalytic degradation of organic compounds, but the effects disappear with decreasing KOH concentration. Alternatively, when Li ions are inserted into non-annealed TNTs followed by post-annealing, the enhanced Li^+ effects are preserved even in circum-neutral pH conditions.

2. Experimental

2.1. Preparation of bare and Li-inserted TiO_2 nanotubes

TNTs were prepared by following a modified anodization method of titanium (Ti) foils in a two-electrode system [10]. A titanium sheet (0.127 mm thick, 99.7%-pure, Aldrich) was cut into small pieces with equal size $1.5 \times 3.0\ cm^2$, which were ultrasonically cleaned in ethanol for 10 min in a sonicaiton bath (WiseClean, 40 kHz, 100 W) and rinsed with deionized water. A couple of a Ti foil piece and a stainless steel plate was immersed in a mixed aqueous solution of NaF (0.28 M) and H_3PO_4 (1.0 M) and a dc voltage of +20 V was applied to the Ti foil (anode) against the stainless steel (cathode) for 4 h with magnetic stirring. Then, the Ti foil piece was annealed at 500 °C for 6 h in the presence of air (pre-annealed TNTs). For Li insertion, the pre-annealed TNTs were immersed in 1 M $LiClO_4$ and negative potentials ranging between −1.0 and −1.7 V was pulsed against a saturate calomel electrode (SCE, reference electrode) for varying times (3–12 s) using a potentiostat (Versastat 3-400). Then, the TNTs were rinsed with deionized water and dried in air (hereafter pre-annealed Li-TNTs). Alternatively, non-annealed TNTs were used for Li insertion under the same electrochemical condition, and then they were annealed at 500 °C for 6 h in the presence of air (post-annealed Li-TNTs). For comparison, bare Ti foils were annealed at 500 °C for 6 h to grow TiO_2 nanoparticles on Ti foils (TNPs), followed by Li insertion.

2.2. Photoelectrochemical and photoelectrocatalytic activity tests

The photoelectrochemical activities of TNTs and Li-TNTs were studied in a three-electrode system with SCE and graphite rod as a reference and a counter electrode, respectively, in various electrolytes ($(NH_4)_2SO_4$, Na_2SO_4, or KOH) using a potentiostat (Versastat 3-400). A 150 W-Xenon arc lamp (Ushio 150-MO) equipped with an AM 1.5G air mass filter was used as a light source. The incident photon-to-current efficiency (IPCE) or external quantum efficiency (EQE) was estimated in 1 M KOH with the same three-electrode system using a 300 W-Xenon lamp (Newport Oriel). Monochromatic light was produced by a CS 130 monochromator with a 10 nm-bandpass, and the output power was measured with a silicon photodiode detector (Newport). The IPCE was then calculated from $(1240 \times J_{ph}) \times 100/(P_{light} \times \lambda)$, where J_{ph} (mA/cm^2), P_{light} (mW/cm^2), and λ (nm) refer to the photocurrent density at 1.0 V_{SCE}, photon flux, and wavelength, respectively. For the impedance analysis (Nyquist plots), alternating current (AC) impedance measurements were carried out through application of a bias potential of −0.3 V_{SCE} in 1 M KOH solution with a frequency range of 10 MHz to 0.01 Hz and an AC voltage of 10 mV rms (Gamry Instruments) [31,32]. For the photoelectrocatalytic activity, as-prepared TNTs and Li-TNTs were immersed in aqueous solutions of phenol (50 and 100 μM), triclosan (0.1 mM), and N,N-dimethyl-p-nitrosoaniline (RNO, 0.1 mM), and the AM 1.5-light was irradiated to the front side of the electrodes through the solutions. The concentrations and intermediates of phenol and triclosan were analyzed with a high performance liquid chromatography (HPLC, YL9100). The mixed eluent with distilled water (with 0.1 wt.% phosphoric acid) and acetonitrile (55/45 v/v) was flowed through a C18-inverse column (4.6 mm × 150 mm) at 1 mL/min. RNO was quantified by recording its main absorption band at 440 nm using a UV–vis spectrophotometer (PerkinElmer, Lambda 950) [33].

2.3. Surface characterization

X-ray diffractometer (XRD, Rigaku D/Max-2500) and X-ray photoelectron spectroscopy (XPS, VG scientific, ESCA LAB 220i XL, MgKα source) were employed to examine crystalline patterns and binding states of sample elements, respectively. Inductively coupled plasma (ICP, PerkinElmer Optima 7300DV) was used to quantify inserted Li ions. Field emission scanning electron microscope (FE-SEM, Hitachi S-4800) was also employed to analyze the morphologies of TNTs and Li-TNTs. Photoluminescence spectra were recorded at room temperature using a spectrometer (f = 0.5 m, Acton Research Co., Spectrograph 500i, U.S.A.) equipped with an intensified photodiode array detector (Princeton Instrument Co., IRY1024, U.S.A.). A He-Cd laser (Kimmon, 1 K, Japan)

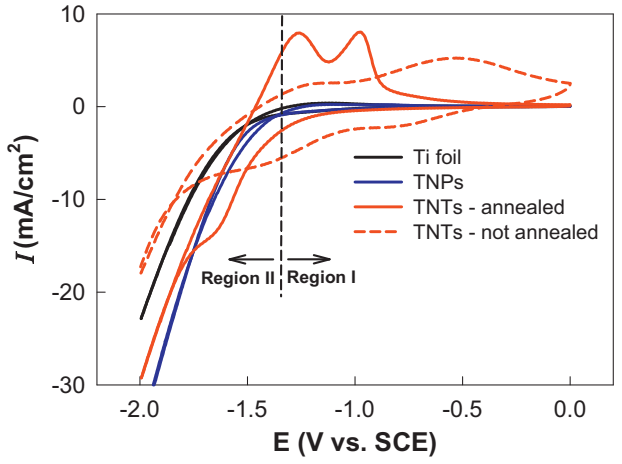

Fig. 1. Cyclic voltammograms of untreated Ti foil, TiO_2 nanoparticles (TNPs), and TiO_2 nanotubes (TNTs) in 1 M $(NH_4)_2SO_4$ (pH 7). Scan rate: 0.1 V/s.

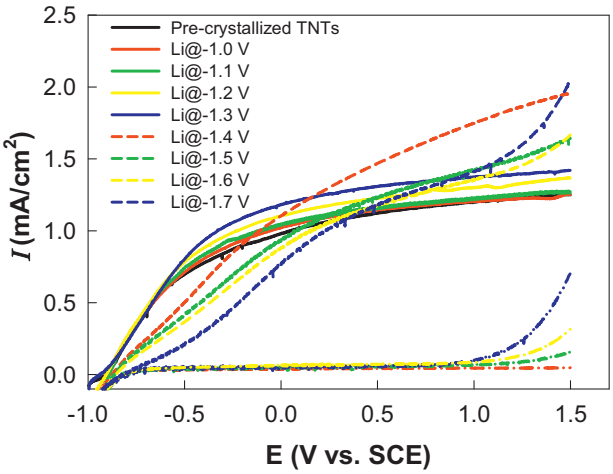

Fig. 2. Linear sweep voltammograms (LSVs) of bare and Li-inserted TNTs in 1 M KOH. For Li insertion, TNTs that were pre-annealed at 500 °C for 6 h were biased to the potentials (as indicated in legend) for 3 s in 1 M $LiClO_4$, washed with deionized water, and used for LSVs.

with a wavelength of 325 nm and power of 50 mW was utilized as the excitation light source [34,35].

3. Results and discussion

3.1. Photoelectrochemical behavior of Li-inserted TiO_2 nanotube arrays

Fig. 1 shows the cyclic voltammograms of an untreated Ti foil, TiO_2 nanoparticles (TNP), and TiO_2 nanotube arrays (TNTs) in 1 M $(NH_4)_2SO_4$ at pH 7. The Ti foil and TNPs produce insignificant anodic currents up to 0 V_{SCE}, whereas substantially high cathodic currents flow from at ~ −1.4 V_{SCE} due to proton reduction (reaction (2)) as well as Ti^{4+} reduction (reaction (3)) [36–39]. A larger cathodic current with TNPs compared to Ti foil may result from the additional reduction pathways of the protons coordinated to TiO_2 (e.g., titanol groups) and/or TiO_2 created on Ti.

$$2H^+ + 2e^- \rightarrow H_2; E^\circ = -0.654\,V_{SCE} \text{ at pH } 7 \quad (2)$$

$$Ti^{4+} + xe^- \rightarrow Ti^{(4-x)+}; x = 1, 2, 3 \quad (3)$$

On the other hand, non-annealed TNTs exhibits two reversible peaks at $E_{1/2}$ ~ −0.65 ($E_{p,a}$ ~ −0.55 V_{SCE}; $E_{p,c}$ ~ −0.75 V_{SCE}) and −1.35 V_{SCE} ($E_{p,a}$ ~ −1.3 V_{SCE}; $E_{p,c}$ ~ −1.4 V_{SCE}). Annealed TNTs (at 500° for 6 h) also shows one reversible peak at $E_{1/2}$ ~ −1.5 V_{SCE} ($E_{p,c}$ ~ −1.6 V_{SCE}; $E_{p,a}$ ~ −1.35 V_{SCE}) and one irreversible anodic peak ($E_{p,a}$) at ~ −1.0 V_{SCE}. These peaks are uniquely found in TNTs and result most likely from the tubular structure. In this study, the potential regions of −1.35 ~ 0 V_{SCE} and −1.7 ~ −1.35 V_{SCE} are arbitrarily assigned to region I and II, respectively. TNTs has diverse TiO_2 surfaces including bottom, inter-wall, and mouth, and their physicoelectrochemical properties appear to be different [10,39]. When a negative potential is applied to TiO_2, an accumulation layer is created. Because mouth TiO_2 is in direct contact with electrolyte and most energetic in terms of geometric configuration, the effect of applied bias on its electrochemical behavior is most significant. In this regard, the peaks found in the region I are related to redox behavior (Ti^{4+}/Ti^{3+}) of mouth and/or wall TiO_2. On the other hand, the peaks in the region II are associated to redox behavior of bottom TiO_2. Macak et al. also proposed that the electrochemical bias of TNTs at −1.45 V_{SCE} reduces selectively Ti^{4+} of bottom TiO_2 in TNTs [39], being consistent to our speculation.

On the basis of the above electrochemical behavior of TNTs, negative potential pulses in the range of −1.0 and −1.7 V_{SCE} were applied to pre-annealed TNTs for 3 s in 1 M $LiClO_4$ to induce Li^+-coupled electron transfer. The samples were then analyzed with linear sweep voltammograms in 1 M KOH electrolyte (Fig. 2). Inserted Li ions are reversibly exchanged with protons (reaction (4)) and the highly alkaline electrolyte (pH ~13.5) is used to inhibit Li^+ liberation from TNTs.

$$Li_xTiO_2 + H^+ \rightarrow H_xTiO_2 + Li^+ \quad (4)$$

Two obviously different types of voltammograms were obtained as shown in Fig. 2. The first type (Li ion insertion at −1.0 ~ −1.3 V_{SCE}, region I) is similar to bare TNTs in the voltammogram shape. The photocurrents of this type increase rather linearly at negative potential range and reach plateau at around ~0 V_{SCE}. In addition, the photocurrents become larger in entire potential range as Li ion insertion potential is more negative. The second type (Li ion insertion at −1.4 ~ −1.7 V_{SCE}, region II) exhibits different voltammogram shapes. Li-TNTs with insertion potential of −1.4 V_{SCE} generates reduced photocurrents at E < ~0 V_{SCE} yet much higher photocurrents at E > ~0.5 V_{SCE}. As Li ion insertion potential decreases step-wisely to −1.7 V_{SCE}, the linear-fashioned voltammograms are obtained and photocurrents do not reach plateau even at high positive potentials. Also, significant amount of dark currents are generated from at ~1.0 V_{SCE} with more negative Li ion insertion potential, likely resulting from water oxidation (reaction (5)).

$$2H_2O \rightarrow O_2 + 4H^+ + 4e^- \quad (5)$$

The effect of the insertion period was also examined under the insertion potential of −1.4 V_{SCE} (Fig. S1). It is found that the insertion period of 1–3 s enhances the PEC activity of TNTs whereas the longer period of 4–11 s reduces the activity.

To understand the effect of Li ion insertion on the photoelectrochemical behavior of TNTs, two hypotheses are proposed as follows. First, most photoevents occur on mouth TiO_2, while bottom TiO_2 has a greater degree of charge recombination [10]. Mouth TiO_2 plays important roles of absorbing photons and creating photocharges. Second, Li ions can be inserted selectively in tubular structure by varying negative potential pulses (region I vs. region II) [39]. As Li ion insertion potential pulses (3 s) shift from −1.0 V_{SCE} to a negative direction in $LiClO_4$, a primary electrochemical reduction of Ti^{4+} occurs at mouth TiO_2. However, the degree of Li ion insertion appears to be small because the reduction currents in the region I are insignificant (Fig. 1). According to scanning electron microscopic images (Fig. 3), a typical wall thickness of TNTs is around 10 nm, much narrower than a few tens of nanometers-thick

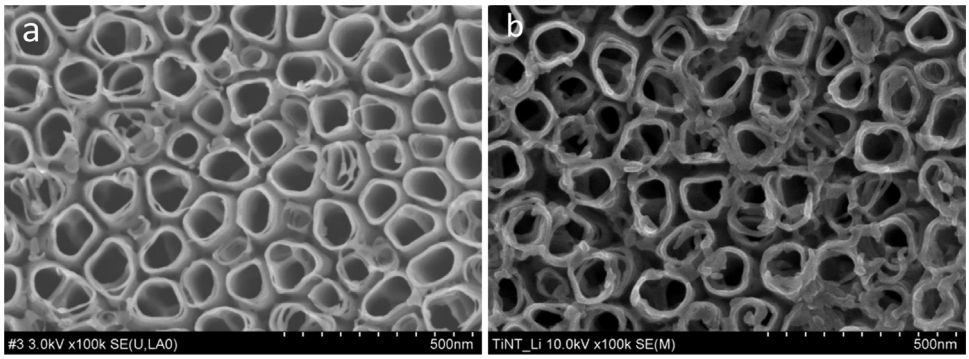

Fig. 3. SEM images of (a) bare and (b) Li-inserted TNTs ($-1.4\,V_{SCE}$ for 3 s in 1 M $LiClO_4$).

surface charge layer of TiO_2 [1]. Under this condition, created surface charge layer is very thin and band bending is insignificant, resulting in the plateau of photocurrent generation at less positive potential biases (see LSVs of Li-TNTs prepared in the region I in Fig. 2). More positive biases neither inhibit charge recombination (reaction (7)) nor enhance interfacial charge transfer effectively (reaction (6)) because the overall reaction may be limited by number of incident photons (photon-limited reaction). When the Li^+ insertion potential arrives at $-1.4\,V_{SCE}$, cathodic currents drastically increases with accelerated Li^+ insertion into bottom TiO_2. As the potential is pulsed at $-1.4\,V_{SCE}$ over 3 s and the potential bias further increases from $-1.4\,V_{SCE}$, bottom TiO_2 may be heavily inserted with Li ions and gradually degenerated. Under this condition, bottom Li-TiO_2 display a kind of metallic property and hence heterojunction semiconductor/metal may be created. A gradual appearance of dark anodic currents at $\sim 1.0\,V_{SCE}$ confirms the metallic property of TiO_2 (Fig. 2). It is uncertain whether Li^+ insertion of mouth TiO_2 is beneficial or not in PEC activity of TNTs because the charge separation at mouth TiO_2 is relatively efficient than that at bulk TiO_2. However, a localized Li^+ insertion to the bottom is important for high PEC activity because the bottom Li-TiO_2 can inhibit the recombination of photogenerated charge carriers transported from mouth TiO_2 (reaction (8)). Inhibited reaction between electrons and Li-TiO_2 (reaction (8)a) is due to energetically high reduction potentials of Li^+ (-3.04 V) and Ti^{3+} (-2.3 V). Meanwhile, hole reaction (reaction (8)b) is also inhibited because one-electron deficient Ti charge (Ti^{3+}) is compensated with Li^+ ions.

$$TiO_2 + h\nu \rightarrow h^+ + e^- \quad (6)$$

$$e^- + \rangle Ti^{IV}\text{-}OH \rightarrow \rangle Ti^{III}\text{-}OH\,(\text{electron trap/transfer}) \quad (6a)$$

$$h^+ + \rangle Ti^{IV}\text{-}OH \rightarrow \rangle Ti^{IV}\text{-}OH^{\bullet +}\,(\text{hole trap/transfer}) \quad (6b)$$

$$e^- + \rangle Ti^{IV}\text{-}OH^{\bullet +} \rightarrow \rangle Ti^{IV}\text{-}OH\,(\text{charge recombination}) \quad (7a)$$

$$h^+ + \rangle Ti^{III}\text{-}OH \rightarrow \rangle Ti^{IV}\text{-}OH\,(\text{charge recombination}) \quad (7b)$$

$$e^- + \rangle Li^{I}\text{-}Ti^{III}\text{-}OH \rightarrow \times\,(\text{inhibition of recombination}) \quad (8a)$$

$$h^+ + \rangle Li^{I}\text{-}Ti^{III}\text{-}OH \rightarrow \times\,(\text{inhibition of recombination}) \quad (8b)$$

3.2. Characterization of Li-inserted TiO_2 nanotube arrays

Li ion insertion little changes the surface morphology of TNTs with pore diameter of ~100 nm and wall thickness of ~10 nm (Fig. 3). No side images were taken for both samples, but they may be similar because TNTs were pre-crystallized (annealed) at 500 °C and Li^+ insertion is a mild and reversible process. The presence of inserted Li ions in Li-TNTs (Li^+ insertion at $-1.4\,V_{SCE}$) was also examined with XPS but Li signals are very weak or sometimes not observed (Fig. S2a) likely due to trace level of Li content and/or inhomogeneous Li distribution (e.g., bottom and wall). Increase in Li^+ insertion time to 5 min generates a Li 1s band yet with weak intensity. Because electrochemically inserted Li ions are balanced with Ti^{3+} in overall charge, XPS spectra for Ti 2p were also examined. The binding energy of Ti 2p is not changed by Li^+ insertion for 3 s. However, the 5 min-sample exhibits a Ti 2p band slightly shifted to lower binding energy with ~0.03 eV (Fig. S2b), indicating that Ti^{4+} is partially reduced to Ti^{3+} [26]. To present a direct evidence of and quantify inserted Li ions, Li ions are withdrawn by immersing Li-TNTs (geometry area: 3 cm^2) in 1 M HCl for 24 h (reaction (4)). ICP-MS analysis indicates that Li ions of ca. 1.7 μmol/cm^2 are inserted into TNTs. Assuming that there are 3–4 Ti atom sites per 1 nm × 1 nm TiO_2 surface [40,41] and Li ions are coordinated to Ti^{3+} at a ratio of 1:1, TiO_2 surface of 3 cm^2 can have ~10^{15} sites for Li ions. This value is three orders of magnitude smaller than that of actually inserted Li ions (1.7×10^{-6} mol × 6.02×10^{23}/mol ≈ 10^{18}-Li^+). This discrepancy can be explained with the followings. First, actual TiO_2 surface area (Ti^{4+} sites) that can be coordinated to Li ions is much larger. This is straightforwardly reasonable because the tubular structure of TNTs should provide much enlarged surface area than the plain structure. Second, Li ions are located not only on surface but also in bulk. If Li^+ diffusion and insertion kinetics is so fast, a substantial amount of Li ions can be inserted even into a deep interior in a few seconds.

To examine the effect of Li^+ insertion on photogenerated charge recombination of TNTs (reaction (8)), photoluminescence (PL) emission spectra are obtained by excitation at 325 nm. TNPs exhibits two broad emission bands at around 500 and 850 nm (Fig. 4: see Fig. S3 for resolved PL bands). The high energy band (~500 nm, corresponding to ~2.5 eV) originates from excited anatase TiO_2 while the near-infrared emission (~850 nm) results from excited rutile TiO_2 [34,42,43]. XRD analysis confirms that anatase and rutile phases coexist in TNPs (Fig. S4). This mixed phase is also found in TNTs and Li-TNTs (Fig. S4). Hence the two broad emission bands are also shown at TNTs and Li-TNTs although their exact positions are different from each other as well as from those of TNPs. The band position of the near-infrared band is almost same for all three samples because it is related to the intrinsic defects in rutile TiO_2 (~1.5 eV) [43]. On the other hand, the high energy band is red-shifted by over 100 nm in TNTs. As compared to TNPs, TNTs have diverse surface (bottom, wall, mouth, etc.) and hence they should have more surface (defect) states and/or oxygen vacancies. These states and vacancies induce multiple charge trap/recombination pathways and consequently change the trap/recombination events occurring in TNPs. As a result, the high energy band disappears and a low energy band centered at ~670 nm appears instead in TNTs. This low energy band seems to be overlapped with another band at ~580 nm, implying an emission band therein (Fig. S3). In the case of

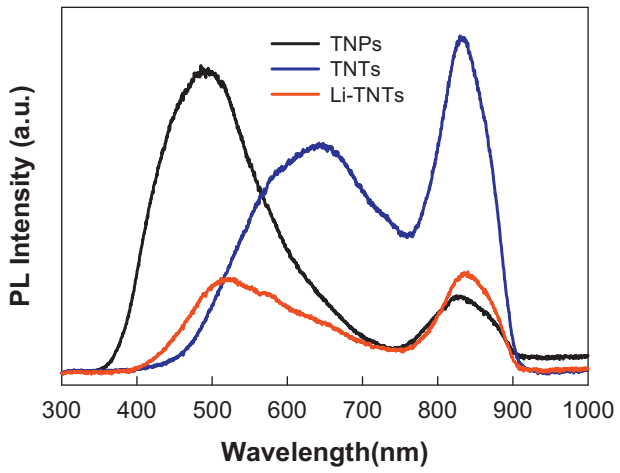

Fig. 4. Photoluminescence (PL) emission spectra of TNPs, TNTs, and Li-TNTs (−1.4 V_{SCE} for 3 s in 1 M $LiClO_4$). For resolved spectra, see Fig. S3.

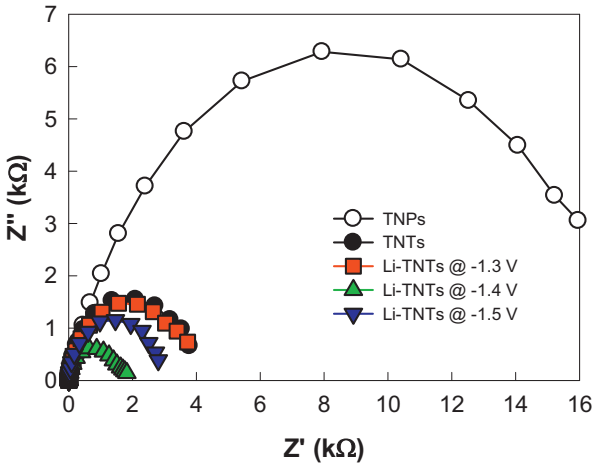

Fig. 6. Electrochemical impedance spectroscopy results for TNPs, TNTs, and Li-TNTs in 1 M KOH.

Li-TNTs, a broad high energy band with a tail is found at ~520 nm, which is resolved into three sub-bands centered at 510, 580, and 650 nm. Emission bands of TiO_2 in the range of 500–600 nm are very sensitive to the presence of cations (Li^+, Na^+, Ce^{4+}, etc.) [44,45], indicating that the high energy band is influenced by Li^+ insertion. It should be noted that Li insertion substantially reduces the overall luminescence intensity of TNTs. This suggests that the charge recombination process is highly inhibited by Li^+ insertion. Because visible luminescence is primarily associated with oxygen vacancies [43,46], the reduced emission intensity further indicates that Li^+ insertion prevents creation of oxygen vacancies (or dangling oxygen) likely due to formation of ⟩Ti-O-Li or charge balance.

To quantify the effect of Li^+ insertion on the charge transfer and recombination, incident photon-to-current-efficiency (IPCE) is analyzed for bare and Li-TNTs in 1 M KOH electrolyte (Fig. 5). IPCE of bare TNTs is 20–28% in the range of $\lambda < 340$ nm, and decreases to zero at ~390 nm. Upon Li^+ insertion at −1.3 V_{SCE}, IPCE is enhanced to ~50% in the range of $\lambda < 340$ nm and further increases to nearly 70% at 320 nm with Li^+ insertion at −1.4 and −1.5 V_{SCE}. A 2.5 fold-improved IPCE by Li^+ insertion is very impressive in that the insertion is highly facile and rapidly completed in 3 s. This indicates that inserted Li^+ effectively retards charge recombination and makes photogenerated electrons collected more efficiently. This in turn implies that charge transfer efficiency can be enhanced by Li^+ insertion. Therefore, electrochemical impedance spectroscopy for

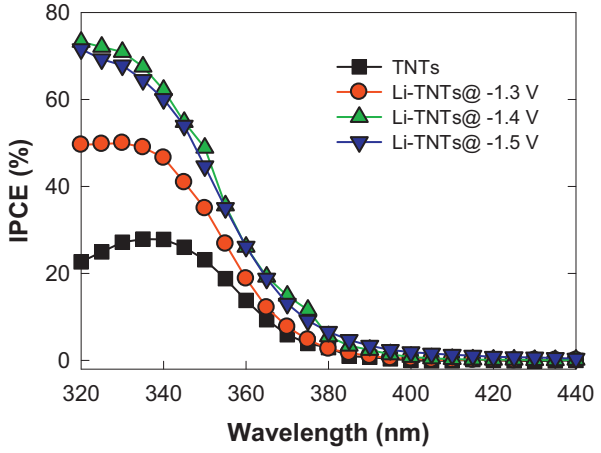

Fig. 5. IPCE for bare TNTs and Li-TNTs in 1 M KOH. Li ions were inserted at −1.3, −1.4, and −1.5 V_{SCE} for 3 s in 1 M $LiClO_4$.

TNPs, TNTs, and Li-TNTs was analyzed to examine the effect of Li ions and compare the charge transfer (Fig. 6). TNPs displays a large semicircle with the charge transfer resistance (R_{ct}) of ~5.4 kΩ cm^2, whereas the semicircle size for TNTs is significantly reduced with R_{ct} of ~1.4 kΩ cm^2. Upon Li^+ insertion at −1.3, −1.4, and −1.5 V_{SCE}, R_{ct} values are further decreased to approximately 1.2, 0.85, and 1.1 kΩ cm^2, respectively. This decrease in R_{ct} value is consistent with enhanced IPCE because charge collection should increase as R_{ct} decreases.

Aforementioned results consistently show that Li^+ insertion significantly enhances the photoelectrochemical performance of TNTs. One great challenge that remains, however, is that such enhanced performance is limited to alkaline conditions (e.g., 1 M KOH) due to reversible Li^+ insertion. To overcome the challenge, Li ions were inserted into non-annealed (i.e., non-crystallized) TNTs which was then followed by the annealing process (post-annealed). It is expected that this post-annealing is to make Li^+ irreversibly inserted into TNTs. The cyclic voltammograms of pre-annealed ("Pre") and post-annealed ("Post") Li-TNTs in 0.1 M Na_2SO_4 (pH ~6) were compared as a function of Li insertion potentials (−1.1 ~ −1.5 V_{SCE} in 1 M $LiClO_4$) under AM 1.5-light (Fig. S5; for the voltammograms in the dark, see Fig. S6). It is obvious that the voltammogram shapes of pre-annealed Li-TNTs are similar to that of bare TNTs and the photocurrent values are not enhanced (even slightly decreased) by Li^+ insertion (Fig. 7). This behavior may be ascribed to Li^+ liberation from TNTs at pH 6 (reaction (4)). On the other hand, post-annealed Li-TNTs display enhanced photocurrent generation at $E > \sim 0$ V_{SCE} in the voltammograms (Fig. S5) and over 2-fold higher constant photocurrents than bare TNTs at a bias of 0.5 V_{SCE} (Fig. 7) and 1.0 V_{SCE} (Fig. S7). This enhanced activity is maintained over 10 h in 0.1 M Na_2SO_4 solution (Fig. S8). Hence the Li^+ insertion state in the post-annealed Li-TNTs is relatively stable and H^+/Li^+ exchange may be reduced. For comparison, the photoelectrochemical activity of pre-annealed Li-TNTs is also maintained over 10 h in 1 M KOH solution (Fig. S8), confirming that the Li^+ insertion state is very stable under highly alkaline condition. Cathodic peaks at $E \sim -0.7$ V_{SCE} in the post-annealed Li-TNTs is likely due to presence of Ti^{3+} ($E^\circ = -0.61$ V_{SCE}) [36]. More detailed study on the post-annealed Li-TNTs will be carried out in near future.

3.3. Photoelectrocatalytic activity of Li-TNTs

To examine the effects of Li^+ insertion on the photoelectrocatalytic activity of TNTs, phenol was selected as a model substrate and its time-profiled decay was monitored in 1 M KOH. For this

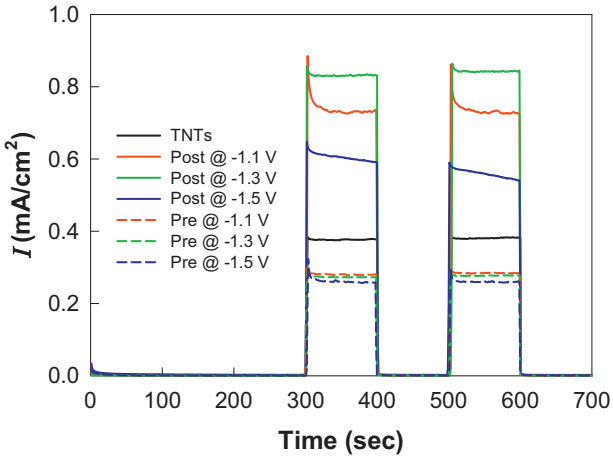

Fig. 7. Time-profiled photocurrent generations from bare TNTs, pre-annealed Li-TNTs (Pre), and post-annealed Li-TNTs (Post) with various Li insertion potentials. Electrolyte: 0.1 M Na_2SO_4 at pH ~6. $E = 0.5\,V_{SCE}$. Pre-annealed Li-TNTs refers to samples prepared sequentially by anodization, annealing, and Li insertion, while post-annealed samples are prepared by anodization, Li insertion, and annealing. For Li insertion, see Fig. 5.

reaction, Li ions were inserted into pre-annealed TNPs and TNTs. As shown in Fig. 8a, Li^+ insertion enhances the degradation kinetics of phenol with TNPs and TNTs. Pseudo-first order rate constants for phenol degradation ($C_t = C_0 \cdot \exp(-kt)$; $C_0 = 0.1$ mM; $R^2 > 0.99$) are

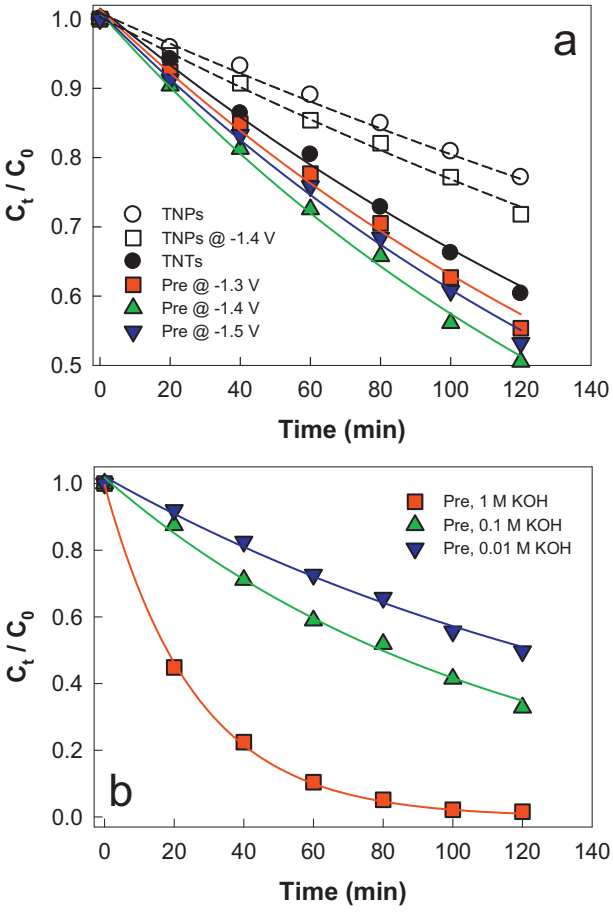

Fig. 8. Photoelectrocatalytic phenol degradation using pre-annealed Li-TNTs (Pre) as a function of (a) Li insertion potentials and (b) KOH concentrations at $1.0\,V_{SCE}$. In (a), 1 M KOH was used as an electrolyte, and TNPs, Li-TNPs, and TNTs were also shown for comparison. The concentrations of phenol were 100 and 50 μM in (a) and (b), respectively. For Li insertion, see Fig. 5.

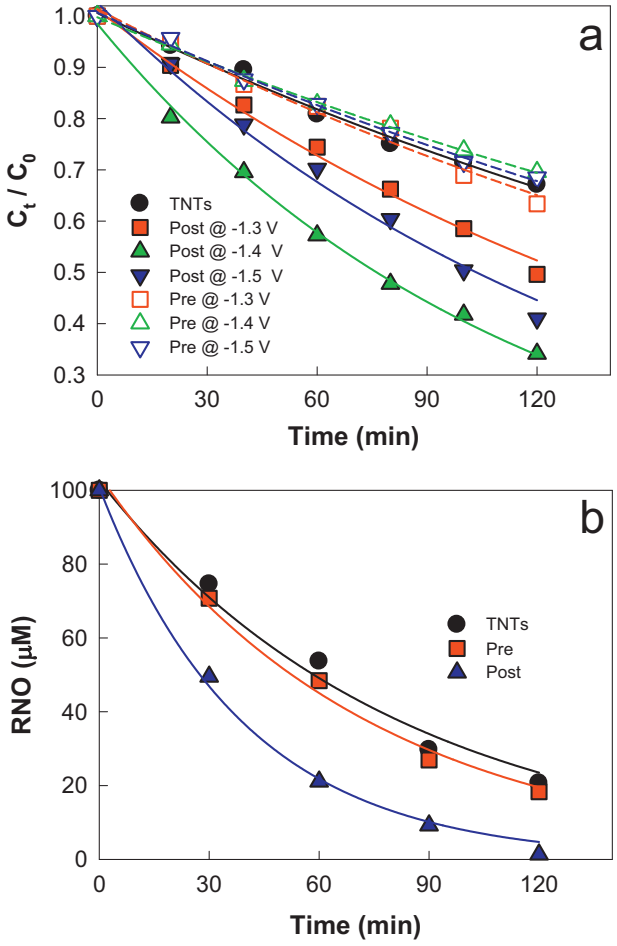

Fig. 9. (a) Photoelectrocatalytic phenol (0.1 mM) degradation and (b) RNO (0.1 mM) degradation using bare TNTs, pre-annealed Li-TNTs (Pre), and post-annealed Li-TNTs (Post) at $1.0\,V_{SCE}$ in 0.1 M Na_2SO_4 (pH ~6). For Li insertion and "Pre & Post", see Fig. 5 and Fig. 7 captions, respectively.

determined to be $\sim 2.3 \times 10^{-3}$ and $\sim 4.2 \times 10^{-3}$ min^{-1}, respectively, which are increased by 17% and 35% by Li^+ insertion at $-1.4\,V_{SCE}$. Other insertion potentials for TNTs also enhance the activity yet with less pronounced effects (13–21%). Similar Li^+ effects are also found for photoelectrocatalytic degradation of trichlosan as a different substrate (Fig. S9). Phenol degradation accompanies the generation of hydroquinone (Fig. S10) with the largest amounts (~12% in 2 h) at Li-TNTs prepared at $-1.4\,V_{SCE}$. The presence of hydroquinone as a primary intermediate suggests that hydroxyl radicals ($OH^\bullet$) are generated from Li-TNTs (reaction (9)). The stability of inserted Li^+ is guaranteed only in highly alkaline condition and therefore the activity of Li-TNTs for phenol should be changed with different KOH concentrations (Fig. 8b). Obviously, as KOH concentration reduces sequentially by a factor of 10 (1, 0.1, and 0.01 M), the rate constants also decreases by a factor of 4.3 and 1.5 ($\sim 3.8 \times 10^{-2}$, $\sim 8.9 \times 10^{-3}$, and $\sim 5.8 \times 10^{-3}$ min^{-1}, respectively). This indicates that inserted Li ions are a controlling factor to maintain the enhanced activity of TNTs.

In terms of practical application, a high photoelectrocatalytic activity limited to alkaline conditions is not desirable and such the activity should be continued in circum-neutral pH conditions. With this in mind, pre-annealed and post-annealed Li-TNTs were compared for their photoelectrocatalytic activities for phenol in 0.1 M Na_2SO_4 at pH ~6 (Fig. 9a). It is obvious that the degradation kinetics of phenol is very similar between bare TNTs and pre-annealed Li-TNTs (Fig. 9a). The absence of Li^+ insertion effect should be

attributed to unfavorable Li^+ insertion state at circum-neutral pH (reaction (4)). On the other hand, post-annealing of Li-TNTs (Li insertion potential of $-1.4\,V_{SCE}$) markedly enhances the kinetics by maximal ~2.6 times. The other two insertion potentials (-1.3 & $-1.5\,V_{SCE}$) also boost the activity of TNTs by 1.6 and 2.0 times. Therefore, the post-annealing appears to be effective to keep the Li^+ insertion effect. Hydroquinone (HQ) and catechol (CC) are detected as primary phenol intermediates (Fig. S11). In contrast to the case of 1 M KOH (Fig. 8 & Fig. S10), detection of catechol may be due to different electrolyte (0.1 M Na_2SO_4). The amounts of hydroquinone and catechol produced are not much different between bare TNTs and pre-annealed Li-TNTs, being consistent with the case of phenol degradation. Meanwhile, post-annealed Li-TNTs produce over 30%-larger amounts of them. Because these intermediates are formed through a hydroxylation of phenol, it is logical to speculate that hydroxyl radicals are generated from irradiated TNTs directly or indirectly. If so, it is also reasonable that the radicals may be more generated at post-annealed Li-TNTs than bare and pre-annealed TNTs. This conjecture is acceptable because Li-TNTs is fully charged and photogenerated holes should be transferred to titanol groups and adsorbed water molecules, creating hydroxyl radicals (reaction (9)).

$$h^+ + \rangle Li^+\text{-}Ti^{3+}\text{-}OH \rightarrow \rangle Li^+\text{-}Ti^{3+}\text{-}OH^{\bullet+} \quad (9a)$$

$$\rangle Li^+\text{-}Ti^{3+}\text{-}OH^{\bullet+} + H_2O \rightarrow \rangle Li^+\text{-}Ti^{3+}\text{-}OH + OH^{\bullet} + H^+ \quad (9b)$$

To examine if this conjecture is true, hydroxyl radicals are quantified in photoelectrocatalytic reactions by a well-established spectroscopic method with a probe molecule (N,N-dimethyl-p-nitrosoaniline, RNO) [33]. It is found that bare TNTs and pre-annealed Li-TNTs exhibit similar RNO quenching kinetics (~8% difference), whereas post-annealed Li-TNTs (Li insertion at $-1.4\,V_{SCE}$) shows ~2-fold faster kinetics (Fig. 9b). This enhancement factor is similar to that for phenol degradation (Fig. 9a), indicating that the Li^+-enhanced activity results most likely from larger generation of hydroxyl radicals.

4. Conclusions

The photoelectrochemical and photoelectrocatalytic performance of TNTs are highly enhanced by the Li ion insertion that is completed only in a few seconds in 1 M $LiClO_4$. Li ion insertion ($-1.4\,V_{SCE}$ for 3 s) enhances the photocurrent generation and the IPCE of TNTs by ~70% and ~2.5 times, respectively. In addition, the photoelectrocatalytic activity for the degradation of phenolic compounds is markedly improved. However, the enhanced Li ion effects are preserved only in a highly alkaline electrolyte and gradually vanish with diluting the alkaline electrolyte due to exchange of inserted Li ions with protons. Simple change of preparation order for Li-TNTs from annealing → insertion to insertion → annealing prevents effectively liberation of inserted Li ions, preserving the Li ion effects even in circum-neutral pH and making Li-TNTs more viable and applicable. Irrespective of preparation methods of Li-TNTs, the Li ion insertion effect can be attributed to the inhibition of charge recombination mostly occurring in electron and hole-trapped sites ($\rangle Ti^{3+}$-OH and $\rangle Ti^{4+}$-$OH^{\bullet+}$, respectively). Because electrochemically created Ti^{3+} is compensated by inserted Li^+ in charge (Li^+-Ti^{3+}-OH), the photogenerated electrons are collected more effectively, while the photogenerated holes are simultaneously transformed into hydroxyl radicals. Li-TNTs with high photoelectrochemical and photoelectrocatalytic activity can work as a platform with reduced charge transfer resistance, promising further and diverse application.

Acknowledgements

This research was supported by the Basic Science Research Programs (No. 2012R1A2A2A01004517, 2010-0002674, and 2011-0021148) and the Korea Center for Artificial Photosynthesis (KCAP) (No. 2012M1A2A2671779) through the National Research Foundation (NRF) funded by MEST, Korea.

Appendix A. Supplementary data

Supplementary data associated with this article can be found, in the online version, at http://dx.doi.org/10.1016/j.apcatb.2013.04.003.

References

[1] C.A. Grimes, G.K. Mor, TiO_2 Nanotube Arrays: Synthesis, Properties and Applications, Springer, New York, 2009.
[2] J.M. Macak, H. Tsuchiya, P. Schmuki, Angewandte Chemie International Edition 44 (2005) 2100–2102.
[3] D.R. Baker, P.V. Kamat, Journal of Physical Chemistry C 113 (2009) 17967–17972.
[4] R. Beranek, H. Tsuchiya, T. Sugishima, J.M. Macak, L. Taveira, S. Fujimoto, H. Kisch, P. Schmuki, Applied Physics Letters 87 (2005).
[5] S.K. Mohapatra, M. Misra, V.K. Mahajan, K.S. Raja, Journal of Physical Chemistry C 111 (2007) 8677–8685.
[6] J.H. Park, S. Kim, A.J. Bard, Nano Letters 6 (2006) 24–28.
[7] T.-S. Kang, A.P. Smith, B.E. Taylor, M.F. Durstock, Nano Letters 9 (2009) 601–606.
[8] M. Paulose, K. Shankar, O.K. Varghese, G.K. Mor, C.A. Grimes, Journal of Physics D: Applied Physics 39 (2006) 2498–2503.
[9] K. Zhu, N.R. Neale, A. Miedaner, A.J. Frank, Nano Letters 7 (2007) 69–74.
[10] T.H. Jeon, W. Choi, H. Park, Journal of Physical Chemistry C 115 (2011) 7134–7142.
[11] Y. Liu, J. Li, B. Zhou, H. Chen, Z. Wang, W. Cai, Chemical Communications 47 (2011) 10314–10316.
[12] Y. Liu, J. Li, B. Zhou, S. Lv, X. Li, H. Chen, Q. Chen, W. Cai, Applied Catalysis B 111–112 (2012) 485–491.
[13] A. Fujishima, X. Zhang, D.A. Tryk, Surface Science Reports 63 (2008) 515–582.
[14] H. Park, Y. Park, W. Kim, W. Choi, Journal of Photochemistry and Photobiology C (2013), http://dx.doi.org/10.1016/j.jphotochemrev.2012.10.001.
[15] S.K. Choi, H.S. Yang, J.H. Kim, H. Park, Applied Catalysis B 121–122 (2012) 206–213.
[16] M. Wagemaker, A.P.M. Kentgens, F.M. Mulder, Nature 418 (2002) 397–399.
[17] R. van de Krol, A. Goosens, E.A. Meulenkamp, Journal of Applied Physics 90 (2001) 2235–2242.
[18] M.P. Cantao, J.I. Cisneros, R.M. Torresi, Journal of Physical Chemistry 98 (1994) 4865–4869.
[19] L. Kavan, J. Rathousky, M. Gratzel, V. Shklover, A. Zukal, Journal of Physical Chemistry B 104 (2000) 12012–12020.
[20] A. Stashans, S. Lunell, R. Bergstrom, A. Hagfeldt, S.E. Lindquist, Physical Review B 53 (1996) 159–170.
[21] H. Xiong, H. Yildirim, E.V. Shevchenko, V.B. Prakapenka, B. Koo, M.D. Slater, M. Balasubramanian, S. Sankaranarayanan, J.P. Greeley, S. Tepavcevic, N.M. Dimitrijevic, P. Podsiadlo, C.S. Johnson, T. Rajh, Journal of Physical Chemistry C 116 (2012) 3181–3187.
[22] F. Fabregat-Santiago, E.M. Barea, J. Bisquert, G.K. Mor, K. Shankar, C.A. Grimes, Journal of the American Chemical Society 130 (2008) 11312–11316.
[23] H.O. Finklea, Semiconductor Electrodes, Elsevier, New York, 1988.
[24] P. Krtil, L. Kavan, D. Fattakhova, Journal of Solid State Electrochemistry 1 (1997) 83–87.
[25] M. Wagemaker, W.J.H. Borghols, F.M. Mulder, Journal of the American Chemical Society 129 (2007) 4323–4327.
[26] S. Sodergren, H. Siegbahn, H. Rensmo, H. Lindstrom, A. Hagfeldt, S.E. Lindquist, Journal of Physical Chemistry B 101 (1997) 3087–3090.
[27] Y. Harima, K. Kawabuchi, S. Kajihara, A. Ishii, Y. Ooyama, K. Takeda, Applied Physics Letters 90 (2007) 103517.
[28] B.H. Meekins, P.V. Kamat, ACS Nano 3 (2009) 3437–3446.
[29] V. Brezova, A. Blazkova, L. Karpinsky, J. Groskova, B. Havlinova, V. Jorik, M. Ceppan, Journal of Photochemistry and Photobiology A 109 (1997) 177–183.
[30] T. Lopez, J. Hernandez-Ventura, R. Gomez, F. Tzompantzi, E. Sanchez, X. Bokhimi, A. Garcia, Journal of Molecular Catalysis A 167 (2001) 101–107.
[31] A. Bak, W. Choi, H. Park, Applied Catalysis B 110 (2011) 207–215.
[32] H. Park, A. Bak, T.H. Jeon, S. Kim, W. Choi, Applied Catalysis B 115–116 (2012) 74–80.
[33] S.Y. Yang, Y.S. Choo, S. Kim, S.K. Lim, J. Lee, H. Park, Applied Catalysis B 111–112 (2012) 317–325.
[34] S.K. Choi, S. Kim, S.K. Lim, H. Park, Journal of Physical Chemistry C 114 (2010) 16475–16480.
[35] S.K. Choi, S. Kim, J. Ryu, S.K. Lim, H. Park, Photochemical & Photobiological Sciences 11 (2012) 1437–1444.

[36] A.J. Bard, R. Parsons, J. Jordan, Standard Potentials in Aqueous Solution, IUPAC, New York, 1985.
[37] L.A. Lyon, J.T. Hupp, Journal of Physical Chemistry 99 (1995) 15718–15720.
[38] N. Sakai, A. Fujishima, T. Watanabe, K. Hashimoto, Journal of the Electrochemical Society 148 (2001) E395–E398.
[39] J.M. Macak, B.G. Gong, M. Hueppe, P. Schmuki, Advanced Materials 19 (2007) 3027–3031.
[40] A. Torrents, A.T. Stone, Environmental Science and Technology 27 (1993) 1060–1067.
[41] H. Park, W. Choi, Journal of Physical Chemistry B 108 (2004) 4086–4093.
[42] S.K. Poznyak, V.V. Sviridov, A.I. Kulak, M.P. Samtsov, Journal of Electroanalytical Chemistry 340 (1992) 73–97.
[43] J. Shi, J. Chen, Z. Feng, T. Chen, Y. Lian, X. Wang, C. Li, Journal of Physical Chemistry C 111 (2007) 693–699.
[44] D.V. Bavykin, S.N. Gordeev, A.V. Moskalenko, A.A. Lapkin, F.C. Walsh, Journal of Physical Chemistry B 109 (2005) 8565–8569.
[45] H. Xin, R. Ma, L. Wang, Y. Ebina, K. Takada, T. Sasaki, Applied Physics Letters 85 (2004) 4187–4189.
[46] F.R. Cummings, L.J. Le Roux, M.K. Mathe, D. Knoesen, Materials Chemistry and Physics 124 (2010) 234–242.